COMPDYN 2011
3rd ECCOMAS Thematic Conference on
Computational Methods in Structural Dynamics and Earthquake Engineering
M. Papadrakakis, M. Fragiadakis, V. Plevris (eds.)
Corfu, Greece, 25–28 May 2011

DEVELOPING FRAGILITY SURFACES FOR MORE ACCURATE SEISMIC VULNERABILITY ASSESSMENT OF MASONRY BUILDINGS

Pierre Gehl[1], **Serigne Sy**[1], **and Darius Seyedi**[1]

[1]BRGM
3 avenue Claude-Guillemin, BP 36009, 45060 ORLEANS Cedex 2, France
e-mail: p.gehl@brgm.fr

Keywords: vulnerability, unreinforced masonry, fragility surfaces, ground-motion parameters

Abstract. *Usual methods for the vulnerability assessment of buildings often result in fragility curves, with respect to one intensity-measure parameter like PGA or spectral displacement. However, the seismic loading is very complex and describing it with one parameter may result in neglecting other significant characteristics of the ground motion [1]. Thus, this study proposes a methodology to develop fragility surfaces, which express the probability of damage with respect to more than one parameter, in order to better account for uncertainties related to the hazard description. The proposed methodology is applied to a model of a two-story unreinforced masonry building (real structure tested on a shaking table by [2]) and the following steps are carried out:*

- *modeling the structure with TREMURI code [3] and static pushover analysis;*
- *developing a set of models with an aleatory distribution of mechanical properties;*
- *based on Latin hypercube sampling, performing hundreds of dynamic analyses (using real and synthetic accelerograms) and assessing the damage level from each analysis;*
- *studying the ground-motion parameters: clustering methods and correlation analyses help to select the appropriate couple of variables to use in the fragility surfaces;*
- *applying the kernel estimation of density in order to get a non-parametrical distribution of damage probability and interpolation into fragility surfaces;*

The proposed framework permits us to choose a couple of ground-motion parameters that are well correlated to the dynamic response of the studied building and, in the same time, are less inter-correlated. The obtained uncorrelated intensity-measures are then used to build unbiased two-variables fragility functions, based on the couple of parameters (PGD and PGA). A comparison between the one-parameter fragility curve and "slices" of the fragility surface shows that the use of a second ground-motion parameter delivers a clearer definition of the vulnerability: the different "slices" can be seen as confidence intervals that can be of great help to public planners, especially in the case of very low probabilities for instance (i.e., extreme events).

1 INTRODUCTION

Current methods of physical vulnerabilty assessment usually result in fragility curves (probability of a given damage level with respect to an intensity-measure parameter), mostly based on parameters such as Peak Ground Acceleration (PGA) or macroseismic intensity. However, it has been recently showed that other ground-motion parameters could be more accurate descriptors of the building fragility. Besides, usual fragility curves neglect the uncertainty introduced by the use of only one parameter to represent the seismic action. Actually, due to the complexity of the seismic loading, accouting for only one parameter may neglect other important characteristics of a seismic time-history, such as the frequency or energy content of the signal.

In the scope of the seismic risk assessment at an urban or regional scale, it is crucial to use accurate information on the vulnerability of common buildings, in order to reduce the scatter in the final results. To this end, the introduction of fragility surfaces (damage probability expressed with respect to two parameters, [1]) instead of single-parameter curves could offer a better knowledge of the vulnerability of a given typology of buildings and provide the public decision-makers with more elaborate data.

Consequently, this study aims at developing a methodology to build analytical fragility surfaces for unreinforced masonry structures: this approach is tested on a two-story brick masonry building. The choice of relevant ground-motion parameters to build the surfaces requires many time-history simulations (unlike a capacity curve approach): thus, the choice of the TREMURI code ([3]) for the structural models has been guided by the use of macrocomponents of masonry panels, which enables faster dynamic calculations than more detailed modeling softwares.

2 STRUCTURAL MODEL WITH TREMURI

2.1 A brief description of TREMURI code

Several post-earthquake observations have shown that unreinforced masonry (URM) panels are composed of rigid undamaged zones, as opposed to vertical or horizontal elements (located between wall openings) that are subjected to shear forces or bending moments. This behavior has led to the developement of a masonry macromodel by [4], and later improved by [5] and [6]: this macroelement has been implemented in the TREMURI code and enables to accurately reproduce the behaviour of a masonry panel, while reducing computation times with respect to more detailed finite-element models. This equivalent-frame approach enables to discretize a masonry wall into several components (vertical elements, named "piers", horizontal ones, named "spandrels", and rigid undamageable zones), represented in Figure 1.

The nonlinear macrocomponent used here takes into account the common in-plane damage mechanisms of a masonry panel (see Figure 2), namely: shear failure (sliding or diagonal) and bending failure.

Damage by shear mechanism is achieved when the shear force of the macroelement reaches the ultimate shear strength, defined by the following criteria ([3]):

- Mohr-Coulomb criteria (for shear sliding):

$$V_u = l' t f_{v0} + \mu N \tag{1}$$

- Turnsek-Cacovic criteria (for diagonal cracking):

$$V_u = lt \frac{1.5\tau_0}{b} \sqrt{1 + \frac{N}{1.5 l t \tau_0}} \tag{2}$$

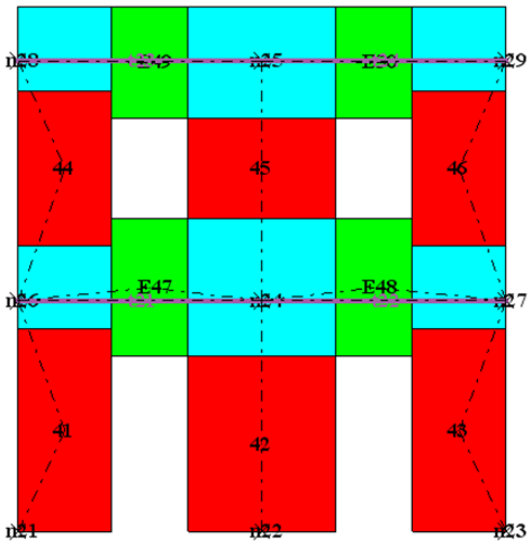

Figure 1: Example of a masonry wall and its openings, modelled into an equivalent-frame. Blue and red elements are respectively the deformable spandrels and piers, whereas the rigid zones are represented in green.

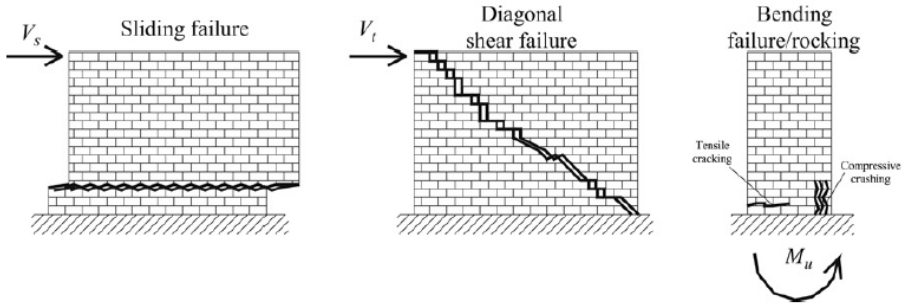

Figure 2: Various damage mechanisms considered for a masonry pier (source - [7])

Where t is the thickness of the macroelement, l its width (l' denoting the actual width of the panel that is subjected to compression), and b a shape factor (height-on-width ratio). The parameter f_{v0} is the shear stregnth without any compression, and τ_0 the shear strength when the tensile strength is reached (first diagonal cracks appearing). Finally, μ is the Mohr-Coulomb friction coefficient and N denotes the axial force that generates compression on the panel.

The ultimate bending moment, representing flexural failure, is defined by:

$$M_u = \frac{l^2 t \sigma_0}{2}(1 - \frac{\sigma_0}{0.85 f_m}) = \frac{Nl}{2}(1 - \frac{N}{N_u}) \tag{3}$$

The ultimate moment depends also on axial compression N, while σ_0 denotes current compression stress and f_m is the compression limit of the masonry.

In the case of 3D modelling, the walls are considered as bearing elements, whereas floors act as horizontal stiffening elements (flexible diaphragms governing the load distribution between the walls). One important assumption in TREMURI is that out-of-plane behavior is not taken into account: it is admitted that such a behavior is negligible due the floor diaphragms and the sound connections between horizontal and vertical components (global box-type behaviour). Thus, in-plane responses of the longitudinal walls (e.g. the ones along the direction of the seis-

mic loading) govern most of the building behaviour: those can take various forms, depending on the type of mechanism (shear or rocking) that is predominant (see Figure 3).

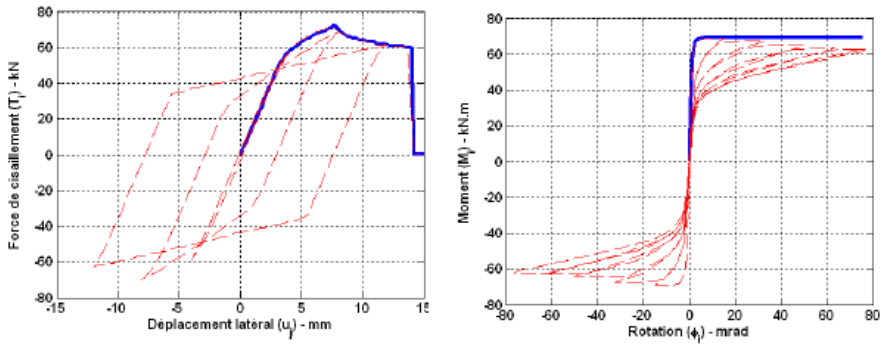

Figure 3: shear (left) and rocking (right) behavior of a single masonry macrocomponent, subject to monotonic (solid line) and cyclic (dotted line) loadings

2.2 Modeling of a two-story URM building

Using the TREMURI macroelement, a building was modeled, based on the results of an experiment in University of Pavia ([2]) on a real scale two-story URM building. The model uses the exact geometry of the real building, while the properties displayed in Table 1 were selected, based on experimental data and common features of brick masonry.

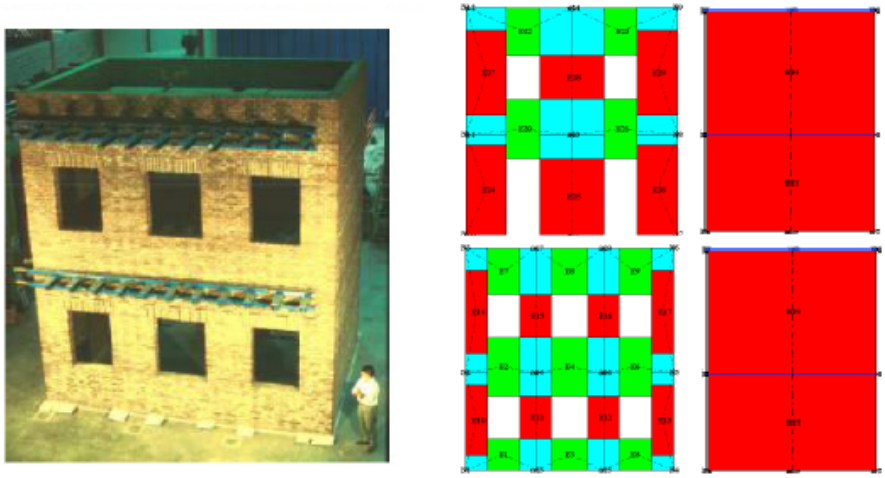

Figure 4: View of the Pavia experiment ([2]) and the corresponding TREMURI model

The structure is around 6m high, with plan dimensions of 6 by 4.4m. As axial forces are a crucial factor in the strength of the masonry, concrete blocks were added on each floor in order to account for live loads: this is traduced into the model with a vertical load of around 250 kN on each floor.

The modal analysis of the 3D model gives the first mode along the length of the building (referred to as the X-direction), for a period $T = 0.149$s (almost 90% of the building mass is concentrated in the first mode along X). The next step is to perform a pushover analysis in

	Parameter	Value
E	Young modulus	3600 MPa
G	Shear modulus	600 MPa
ρ	Density	1800 kg/m3
f_m	Compressive strength	6.2 MPa
f_{sh}	Shear strength	0.23 MPa
D_{sh}	Shear ultimate drift ratio	0.6%
D_{fl}	Rocking ultimate drift ratio	0.8%
μ	Friction coefficient	0.2

Table 1: Mechanical properties of the building model

order to obtain the building global strength and the ultimate top displacement: a progressive lateral force is applied along the X-direction, while the forces are distributed at each floor according to the first mode shape. Based on some previous studies ([8], [9]), it is admitted that the ultimate displacement is reached when the shear force falls down to 80% of its maximum value: using the equal-energy criterion, an idealized bilinear curve is then generated, yielding the elastic-limit point.

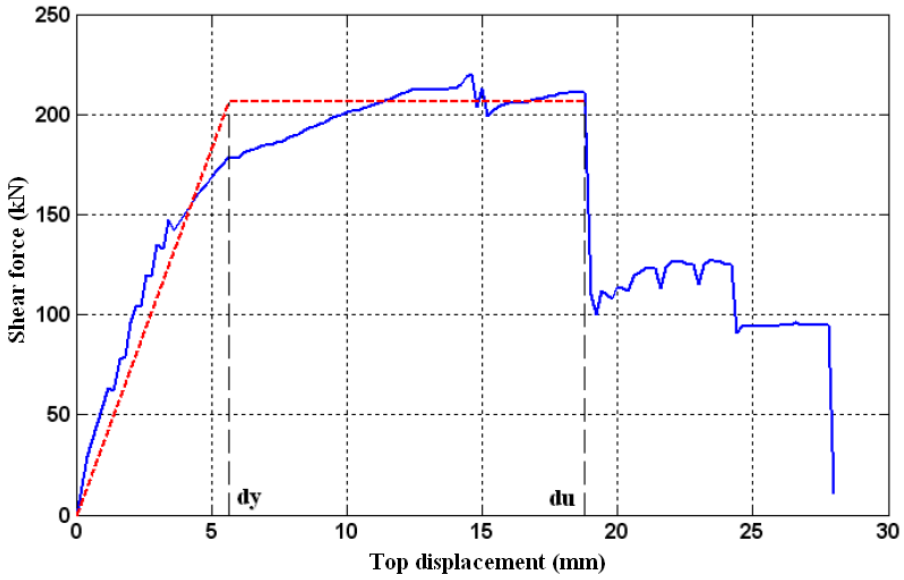

Figure 5: Pushover curve of the building model (solid line), along with the bilinear curve (dotted line). Limit-displacement values $d_y = 5.6$mm and $d_u = 18.8$mm can be identified.

The evaluation of the damage state at the building level is not trivial, as the criteria used to define the local damage level of a macrocomponent cannot be simply extrapolated to a global level. Among the numerous damage indicators available in the literature (index based on hysteretic energy dissipation [10], determinant of the stiffness matrix, maximum strain values at various locations, ...), it is chosen here to use the transient interstory drift ratio (ISDR) or floor displacements because their computation is rather straightforward and many correlations between floor displacement and damage states have been developed. The Risk-UE project ([11]) proposes some relations to link displacements d_y and d_u to the EMS-98 ([12]) damage scale

(see Table 2).

Damage state	Displacement-limit	Value (mm)
Slight	$d = 0.7d_y$	3.94
Moderate	$d = 0.7d_y + 0.05(0.9d_u - 0.7d_y)$	4.59
Extensive	$d = 0.7d_y + 0.2(0.9d_u - 0.7d_y)$	6.54
Very heavy	$d = 0.7d_y + 0.5(0.9d_u - 0.7d_y)$	10.43
Collapse	$d = 0.9d_u$	16.92

Table 2: Correlation between EMS-98 damage states and the transient top displacement, for unreinforced masonry buildings, according to [11]

The recommendations from the FEMA-356 [13] document for unreinforced masonry give some values of transient ISDR corresponding to different levels of safety: 0.1% for S-1 (Immediate Occupancy) and 0.5% for S-3 (Life Safety). The results of the static analysis on the studied building give a top displacement $d = 5.8$mm for S-1 level, and $d = 20.8$ mm for S-3. Even if both damage scales are not to be compared, it appears that the FEMA criteria tend to be much less conservative than the Risk-UE values for this specific building. FEMA criteria are fixed drift ratios that are the same for a generic typology of buildings, whereas the Risk-UE values are based on the strength and the ductility of each model and may be more accurate for specific cases. Thus, the boundaries in Table 2 will be used for the rest of the study.

2.3 Development of variant models

Once the first building model is developed and validated, the uncertainties on the mechanical properties of the brick masonry can be taken into account by deriving a set of variants with respect to the basic model. Those variants are developed by sampling material properties, which are assumed to have a normal distribution. The associated coefficients of variation can be taken from various past studies ([14], [15]) and the distributions of the varying parameters are represented in Table 3.

Parameter	Mean	C.O.V.	St.-Dev. s	Lower bound	Upper bound
E (MPa)	3600	20%	720	2160	5040
G (MPa)	600	20%	120	360	840
f_m (MPa)	6.2	20%	1.24	3.72	8.68
f_{sh} (MPa)	0.23	15%	0.0345	0.161	0.299
D_{sh} (%)	0.6	10%	0.06	0.48	0.72
D_{fl} (%)	0.8	10%	0.08	0.64	0.96

Table 3: Proposed variations of some basic mechanical parameters for the masonry model

For each parameter, some bounds (set at $+/-2s$) prevent from sampling irrelevant values. We choose to generate 20 variant models out of the parametric distribution: a Latin hypercube sampling scheme is used in order to optimize the possible combinations with a reduced number of models. Thus, with 20 models, intervals of 5% can be defined and, for each parameter, an aleatory interval has been picked to sample the value for a given model. This procedure results in a total of 21 structures (one basic model plus 20 variants): for each of them, a pushover analysis is performed in order to identify the boundaries of the EMS-98 damage states.

3 NON-LINEAR DYNAMIC ANALYSES

3.1 Selection of the accelerogram datatset

The dynamic analyses on the models require a large set of seismic time-histories, in order to build consistent fragility functions. First, a sample of 120 records has been selected from the European Strong-Motion Database ([16]): these accelerograms were generated by earthquakes of magnitude (Mw) between 5.3 and 6.3, at a focal depth lower than 30km. These criteria correspond approximately to the kind of earthquakes that are to be expected in Southern France. In order to increase the size of the dataset, another series of signals has been generated, using the non-stationary stochastic procedure proposed by [17], an extension of [18]. This signal generation spans a magnitude range from 4.5 to 6.5, with the epicentral distance comprised between 10 and 100km. Also, for each magnitude-distance combination, the signal is derived for the five Eurocode-8 soil classes, in order to account for the variability in site conditions. Finally, these stochastic simulations have output 657 synthetic accelerograms, resulting in a total of 777 time-histories.

The consistency between real records and synthetic accelerograms has been checked for a wide selection of grond-motion parameters: the overall distribution of the two datasets (mean and standard-deviation) shows good agreement, except for duration-related parameters, which have a tendency to be underestimated in the synthetic signals used here ([17]).

3.2 Simulation scheme and results

The selected accelerograms are now applied at the basis of the structure, along the X-direction. The number of simulations has been optimized and the dataset of 777 accelograms has been divided into 37 groups of 21 records each. Thus, within each group, it is possible to randomly assign each accelogram with one of the 21 models. It is worth noting that the 37 groups were selected by ranking all accelerograms with respect to PGA (ground-motion parameter selected a priori to represent the "nocivity" of the signal): this ensures that each group contains homogeneous signals, and as a result all 21 models are sujected to accelerograms with similar intensity levels.

Then, all non-linear dynamic analyses are carried out and the maximum transient displacement at the top of the building is used to identify the different damage states, based on Table 2. The results of the analyses are summed up in Table 4, in terms of relative percentage of the 777 simulation runs. It appears that more than the half of the simulations have not induced any damage to the structure. About 17% of them induce the collapse, while intermediate levels (e.g. slight to very heavy damage) are clearly underrepresented.

Damage state (EMS-98)	Percentage of runs
None	62.8%
Slight	1.8%
Moderate	5.5%
Extensive	6.1%
Very heavy	6.4%
Collapse	17.4%

Table 4: Distribution of the number of simulations that have reached the different damage states

Using these raw results, fragility curves based on a single intensity-measure parameter (for

instance, PGA, as it is a widely known and usual parameter) can be built. These curves are fitted to a lognormal cumulative distribution function, as shown below:

$$P_k(PGA) = P(damage \geq D_k|PGA) = \phi[\frac{\ln(\frac{PGA}{\mu})}{\sigma}] = \frac{1}{2}[1 + erf(\frac{\ln PGA - \ln \mu}{\sigma\sqrt{2}})] \quad (4)$$

The median μ and the standard deviation σ can be defined using the maximum likelihood method, as proposed by [19]. After an optimisation procedure using the simplex method, the variables for each damage state are displayed in Table 5. The corresponding fragility curves are plotted on Figure 6.

Parameter	Slight	Moderate	Extensive	Very heavy	Collapse
μ	1.1108	1.2466	1.5724	2.1728	2.9359
σ	0.2928	0.3047	0.4146	0.4973	0.4966

Table 5: Estimated medians and standard-deviations for the fragility curves, with respect to PGA

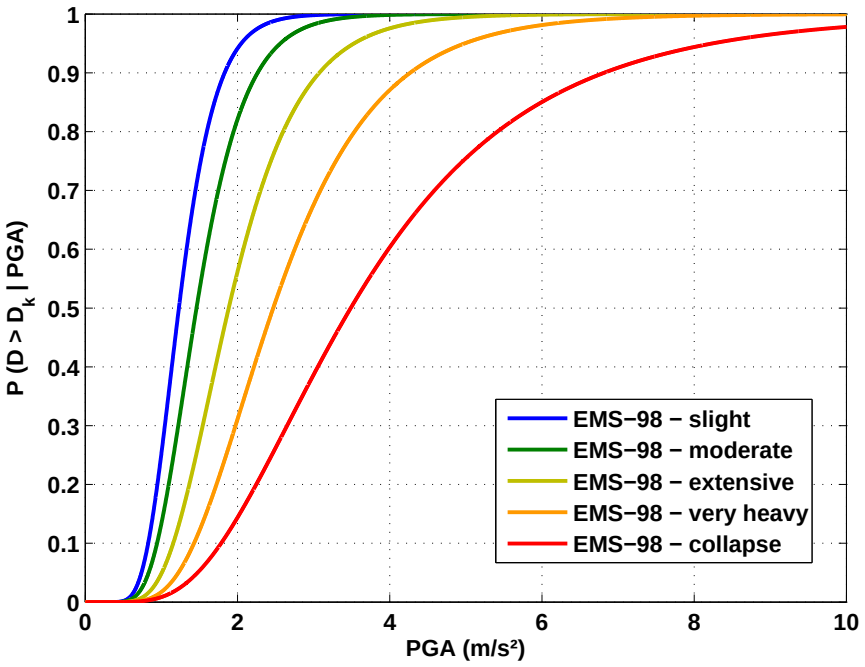

Figure 6: Analytical fragility curves for the studied low-rise URM building, with respect to PGA

4 SELECTION OF GROUND-MOTION PARAMETERS

This section is devoted to the selection of proper ground-motion parameters that could make an adequate couple of IM variables for the fragility surfaces.

4.1 Clustering of ground-motion parameters

From each of the accelerograms used in the simulations, 46 ground-motion parameters have been estimated, ranging from PGA to cyclic and duration parameters or spectral values. The first step is to rank these parameters according to their cross-correlation: The VARCLUS procedure is used to this end. It consists in a succession of principal component analyses and the merging of the parameters with strong correlation into distinct class-variables, or "clusters". This procedure is very helpful to reduce the high number of parameters to only 3 or 4 variables that are representative of the distribution of the studied ground-motion parameters (see Table 6).

Cluster 1	Cluster 2	Cluster 3
PGA	PGV	Duration bracketed rel.
Arias intensity	PGD	Duration uniform rel.
A95	Duration bracketed abs.	Duration significant rel.
SLOPE75	Duration uniform abs.	Nb of effective cycles
SLOPE95	Duration significant abs.	
ARMS	Sd ($T = 0.05$s to $T = 1.25$s)	
ASI	Sa ($T = 0.05$s to $T = 1.25$s)	
Cyclic damage parameters		
Sd ($T = 1.5$s to $T = 5$s)		
Sa ($T = 1.5$s to $T = 5$s)		

Table 6: Generated clusters from the accelerogram dataset and corresponding ground-motion parameters

Some of the ground-motion parameters studied above are not usual ones, and we propose here a very brief description of some of them:

- A95: the level of acceleration which contains up to 95% of the Arias intensity.
- SLOPE75 and SLOPE95: the slope of the Husid plot (e.g. cumulative Arias intensity over time) between 5% and 75% (or 95%) of the total Arias intensity.
- ARMS (Root-mean-square acceleration): the square-root of the integral of squared acceleration over time.
- ASI (Acceleration spectral intensity): the integration of the spectral acceleration between two periods (here, 0.1s and 0.5s).

More details on the way to estimate these IM parameters are given in [20]: various definitions of the duration parameters are provided, along with the different ways to count cycles.

As a result, with only 3 variables remaining, it is more straightforward to study the correlation of the ground-motion parameters with the simulation results. In Table 7, the correlation coefficients between the transient drift and the 3 class-variables are represented.

This first analysis shows that relevant ground-parameters are to be selected from both clusters 1 and 2, whereas cluster 3 is almost uncorrelated to the drift and thus has very little impact on the behavior of the structure.

	Drift	Cluster 1	Cluster 2	Cluster 3
Drift	1	0.7715	0.9043	−0.1054
Cluster 1	-	1	0.8194	−0.0794
Cluster 2	-	-	1	−0.1712
Cluster 3	-	-	-	1

Table 7: Correlation coefficients between the drift obtained from simulations and the class-variables representative of ground-motion parameters

4.2 Selection of the adequate couple of ground-motion parameters

In order to build relevant fragility surfaces, the adequate IM parameters should be both well correlated with the response of the structure (e.g. the drift) and also as uncorrelated as possible between each other. As a result, based on the cluster analysis above, one IM parameter should be selected from cluster 1 and the other one from cluster 2. To this end, we represent in Table 8 all parameters from cluster 1 and 2 that have a correlation coefficient with the drift greater than $R = 0.75$. Also, parameters like cyclic damage, signal duration or SLOPE, are discarded because their computation through usual ground-motion prediction equations is not feasible right now: thus, in the scope of a seismic risk scenario, such IM parameters would be rather useless.

	A95	PGA	Arias Int.	ARMS	Sd1.5s	Sa1.5s	Drift
PGV	0.8657	0.8657	0.8034	0.8280	0.8450	0.8446	0.9107
Sa0.5s	0.8263	0.8233	0.7751	0.7821	0.8173	0.8170	0.9006
Sd0.5s	0.8228	0.8225	0.7748	0.7815	0.8170	0.8167	0.9001
Sa0.075s	0.7978	0.7976	0.7695	0.7559	0.7880	0.7877	0.8822
Sa0.25s	0.8010	0.8046	0.7798	0.7681	0.8049	0.8046	0.8817
Sd0.075s	0.7971	0.7968	0.7687	0.7552	0.7873	0.7869	0.8816
Sa0.1s	0.7954	0.7973	0.7781	0.7618	0.7881	0.7876	0.8814
Sd0.25s	0.8006	0.8041	0.7795	0.7678	0.8045	0.8042	0.8813
Sd0.1s	0.7944	0.7964	0.7776	0.7609	0.7873	0.7869	0.8809
Sd0.75s	0.8435	0.8413	0.7703	0.7933	0.8262	0.8260	0.8713
Sa0.75s	0.8437	0.8416	0.7704	0.7934	0.8263	0.8262	0.8712
Sd1.0s	0.8547	0.8563	0.8064	0.7961	0.8554	0.8552	0.8546
Sa1.0s	0.8551	0.8567	0.8070	0.7963	0.8560	0.8558	0.8541
Sa1.25s	0.8845	0.8805	0.8109	0.8284	0.8876	0.8876	0.8447
Sd1.25s	0.8841	0.8801	0.8111	0.8280	0.8877	0.8876	0.8444
Sa0.05s	0.6758	0.6806	0.7088	0.6717	0.6962	0.6959	0.8204
Sd0.05s	0.6695	0.6745	0.7053	0.6675	0.6909	0.6906	0.8163
PGD	0.6092	0.6132	0.6601	0.6144	0.6095	0.0.6092	0.7739
Drift	0.7902	0.7841	0.7784	0.7582	0.7504	0.7498	1

Table 8: Correlation coefficients between parameters from clusters 1 and 2, and also with the drift

An obvious move would be to choose Peak Ground Velocity (PGV) as the first IM parameter, because of its good correlation with the drift: yet, this parameter is also strongly correlated with all secondary parameters from the other cluster (coefficients R above 0.8) and this would add

no extra information on the seismic vulnerability of the structure. On the other hand, the PGA is quite well correlated with the drift ($R = 0.7841$) and shows also poor correlation (see Figure 7) with the Peak Ground Displacement (PGD) ($R = 0.6132$): as a result, the couple of variables (PGA, PGD) can be considered as good candidates upon which to build the fragility surfaces. One could argue that A95 and PGD would constitute a slightly better couple of parameters: yet, the parameter A95 cannot be easily obtained from ground-motion equations and its use is by far not as common as the PGA. Anyway, in a more physical sense, this means that the vulnerability of this low-rise masonry building can be well represented by both acceleration and displacement-based parameters.

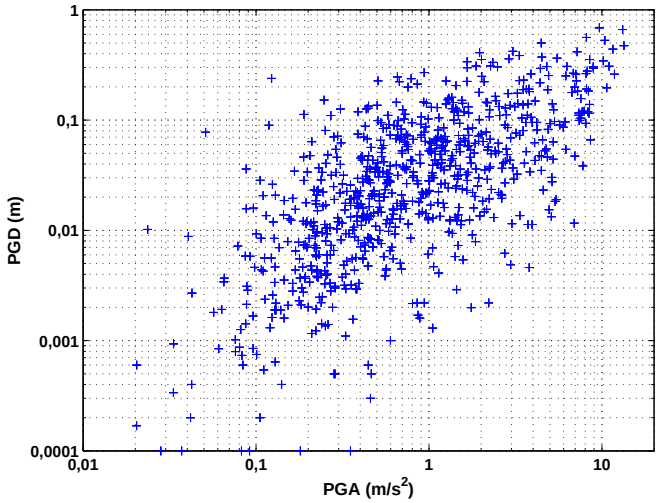

Figure 7: Distribution of the PGA and PGD values for all the accelerograms used in the simulations

5 DEVELOPMENT OF FRAGILITY SURFACES

5.1 Mathematical formulation

While fragility curves are usually represented by well-known and readily parameterizable probability distributions like the lognormal one ([21], [19]), the problem gets more complex for surfaces, where bivariate distributions must be computed. One solution is to use the kernel density estimation procedure (or Parzen-Rosenblatt method), which allows a non-parametric definition of the probability density and is thus applicable to higher-dimension problems ([22]).

Let us consider the data (PGA_i,PGD_i) corresponding to the $n = 777$ accelograms used in the simulations. Then it is possible to write a two-dimensional non-parametric estimator using the kernel density method:

$$f_h(PGA, PGD) = \frac{1}{n.\, h_{PGA,n}.\, h_{PGD,n}} \sum_{i=1}^{n} K(\frac{PGA_i - PGA}{h_{PGA,n}}) K(\frac{PGD_i - PGD}{h_{PGD,n}}) \qquad (5)$$

The function K is the kernel and h is the "window", a parameter similar to the standard-deviation that controls the degree of smoothing of the estimation. K usually takes the functional form of a standard normal distribution:

$$K(x) = \frac{1}{\sqrt{2\pi}} e^{-\frac{x^2}{2}} \tag{6}$$

The window h is estimated through optimisation functions that seek to minimize the error (Mean Integrated Squared Error is used as the metric), depending on the size n of the sample and whether it is homogeneously distributed or not.

According to Table 4, intermediate damage states seem not well represented and the resulting fragility surfaces might suffer from a too large scatter. Therefore it is decided to develop only the surfaces for the damage states "slight" and "collapse". If we want to build the fragility surface corresponding to the slight damage level, we have to define first the estimator $f_{h,all}$ for the whole data (the 777 points), as well as the estimator $f_{h,slight}$ that gives the density of the records reaching or exceeding the slight damage state (e.g. 289 points). Then, the probability of the structure reaching this damage state is given by:

$$P1(PGA, PGD) = \frac{289 f_{h,slight}}{777 f_{h,all}} = \frac{h_{PGA,777} . h_{PGD,777}}{h_{PGA,289} . h_{PGD,289}} . \frac{\sum_{i=1}^{289} K(\frac{PGA_i - PGA}{h_{PGA,289}}) K(\frac{PGD_i - PGD}{h_{PGD,289}})}{\sum_{i=1}^{777} K(\frac{PGA_i - PGA}{h_{PGA,777}}) K(\frac{PGD_i - PGD}{h_{PGD,777}})} \tag{7}$$

The estimators are normalized by the size of the sample in order to get a proper cumulative distribution function, comprised between 0 and 1. In order to compare two estimators, both windows h should be the same so that densities are kept homogeneous. A high value of h denotes a small size sample or with strong disparities. Therefore the highest value of h is chosen, the limiting factor being the lowest quality estimator. We can then define:

$$\begin{aligned} h_{PGA} &= max[h_{PGA,777}; h_{PGA,289}] \\ h_{PGD} &= max[h_{PGD,777}; h_{PGD,289}] \end{aligned} \tag{8}$$

As a result, the probability of damage can finally be written as:

$$P1(PGA, PGD) = \frac{\sum_{i=1}^{289} K(\frac{PGA_i - PGA}{h_{PGA}}) K(\frac{PGD_i - PGD}{h_{PGD}})}{\sum_{i=1}^{777} K(\frac{PGA_i - PGA}{h_{PGA}}) K(\frac{PGD_i - PGD}{h_{PGD}})} \tag{9}$$

It is then possible to plot this bivariate probability function and represent it as a fragility surface (see Figure 8).

5.2 Interpretation of the results

The main motivation for developing fragility surfaces lies in a better definition of the level of seismic aggression, hence maybe a reduction of the uncertainty related to the hazard level description (usually represented by a single parameter like PGA). In order to confront both approaches, we transpose a fragility surface into 2D curves by isolating "slices" that represent the probability with respect to one IM parameter, while keeping the second one constant. An example is displayed in Figure 9, for the "slight" damage level.

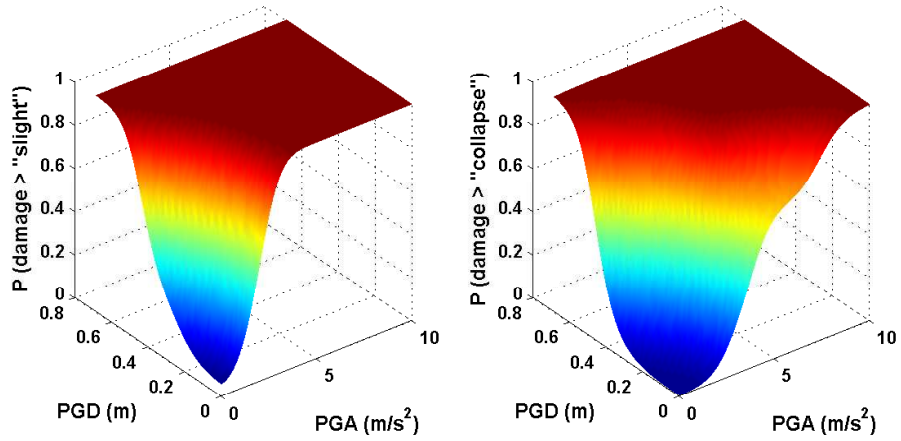

Figure 8: Fragility surfaces of the studied structure, for levels of damage "slight" and "collapse"

Firstly, it can be noticed that the use of a second parameter (e.g. PGD, an easily accessible variable through ground-motion prediction equations) induces a steady increase of the damage probability. For instance, in the case of small accelerations (PGA lower than $0.5m/s^2$), the single-parameter curve shows almost zero probability of damage: however, the fragility surfaces indicates that if this ground-motion is generated along with important ground deformation (e.g. $PGD = 0.1$m or 0.2m), then there is actually a non negligible probability of damage (between 10% and 20%).

The single-parameter curve does not account for the different possible values of PGD, therefore there is a tendency to neglect physical damaging phenomena related to ground displacements: the black line in Figure 9 hides indeed the epistemic uncertainty due to the absence of the second IM parameter. On the contrary, this epistemic uncertainty is well quantified by the fragility surface, which "slices" can be seen as confidence intervals on the damage probability. According to [23], most decision makers in the field of natural risks are likely to deal with confidence intervals rather than averaged probabilities, especially in the case of rare or extreme events (on the extremities of the distribution). Let us take the example of strong accelerations (e.g. $PGA = 2.5m/s^2$): the single-parameter curve yields a damage probability of 99%. Let us assume that for this level of acceleration, it is possible to determine the PGD value with a confidence interval between 0.1m and 0.3m: thus, the fragility surface can show that the damage probability will be comprised between 95% and 100%, linking directly the uncertainty on a ground-parameter to the epistemic uncertainty on the fragility.

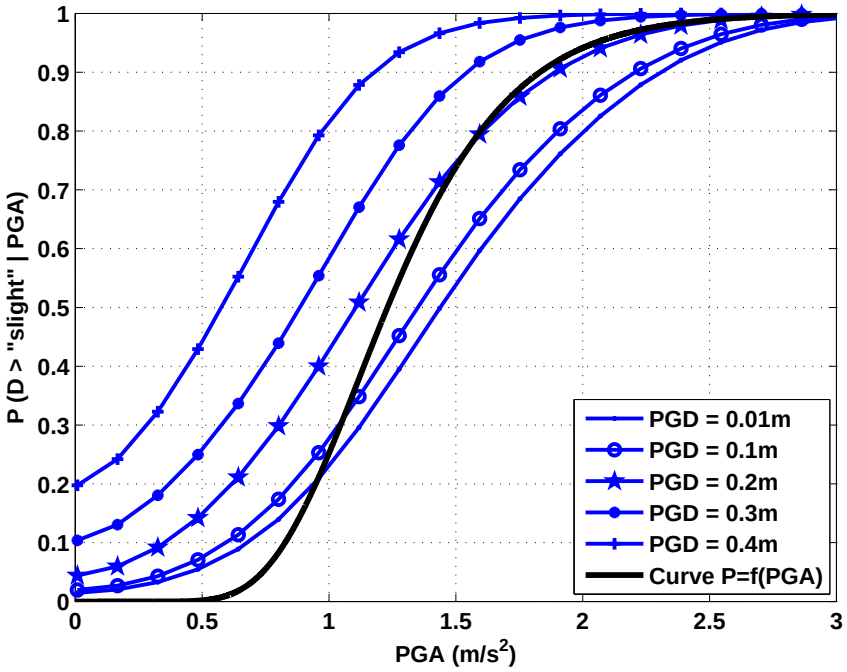

Figure 9: Single-parameter fragility curve (black line) compared to slices of the fragility surface

6 CONCLUSIONS

Starting from the use of the TREMURI code and its masonry macroelements, this study has proposed a procedure to derive analytical fragility surfaces through non-linear dynamic simulations, in the specific case of a low-rise URM building. The first steps of this procedure – such as the structural modelling, the static analyses to identify displacement boundaries for damage states, the selection of an accelerogram dataset and the time-history simulations – are the ones usually performed to develop single-parameter fragility curves.

Yet, in the case of fragility surfaces, the IM parameters are to be chosen carefully: both parameters should be well correlated with the response of the structure (e.g. top displacement or drift) in order to provide an efficient representation of the damage probability. However, there is also no point in choosing two IM paramters that are well correlated with each other, as such a surface would show nothing more than a single-parameter curve. To this end, a procedure of parameter selection has been proposed: it is based on the analysis of various ground-motion parameters and their ranking into clusters of variables. Then, a final judgement is made on the basis of correlation coefficients, in order to select the adequate couple of IM parameters.

Fragility surfaces, or in other words biviariate probability functions, have been built using a non-parametric probability density, through the use of kernel density estimators. The results have shown that these fragility surfaces can be useful in the sense that they provide a more complete description of the seismic aggression: as a result, the probability values obtained through

the surfaces add another layer of information (the epistemic uncertainty related to the second IM parameter) and allow the definition of confidence intervals for the damage probabilities, which may be more interesting for decision makers than averaged probability values.

ACKNOWLEDGEMENTS

The work presented in this article has been supported by BRGM funds and by French Research National Agency (ANR) through PGCU-2007 program (project EVSIM, A mechanical approach to Evaluate Seismic Vulnerability of Masonry structures). We thank the providers of the strong-motion and the structural data used. In addition, we thank Dr Guillaume Pousse for sending us his computer program to simulate strong-motion records using his method. We thank also Prof. Sergio Lagomarsino for sharing with us the research and development version of TREMURI.

REFERENCES

[1] D. Seyedi, P. Gehl, J. Douglas, L. Davenne, N. Mezher, S. Ghavamian, Fragility surfaces for modelling the seismic vulnerability of reinforced concrete structures. *Earthquake Engineering and Structural Dynamics*, **39**, 91–108, 2010.

[2] G. Magenes, G.R. Kingsley, G.M. Calvi, Static testing of a full scale, two-story masonry building: test procedure and measured experimental response, in Experimental and numerical investigation on a brick masonry building prototype. *Report 3.0 CNR-GNDT Numerical Prediction of the experiment: 1.1 - 1.41*. 1995.

[3] S. Lagomarsino, A. Penna, A. Galasco, *TREMURI Program: Seismic Analysis Program for 3D Masonry Buildings*. University of Genoa, `http://www.stadata.com/`, 2006.

[4] K. Gambarotta, S. Lagomarsino, On dynamic response of masonry panels. *Proceedings of National Conference "Masonry mechanics between theory and practice"*, Messina, Italy, 1996.

[5] A. Penna, *A macro-element procedure for the non-linear dynamic analysis of masonry buildings*. PhD Dissertation, Politecnico de Milano, Italy, 2002.

[6] A. Galasco, S. Lagomarsino, A. Penna, On the use of pushover analysis for existing masonry buildings. *First European Conference on Earthquake Engineering and Seimology*, Geneva, Switzerland, September 3-8, 2006.

[7] V. Mallardo, R. Malvezzi, E. Milani, G. Milani, Seismic vulnerability of historic masonry buildings: a case study in Ferrara. *Engineering Structures*, **30**, 2223–2241, 2008.

[8] M.Y. Kaltakci, M.H. Arslan, H.H. Korkmaz, M. Öztürk, An investigation on failed or damaged reinforced concrete structures under their own weight in Turkey. *Engineering Failure Analysis*, **14**(6), 962–969, 2007.

[9] Y. Lu, H. Hao, P. Carydis, H. Mouzakis, Seismic performance of RC frames designed for three ductility levels. *Engineering Structures*, **23**, 537–547, 2001.

[10] Y.J. Park, A.S. Ang, Seismic damage analysis of reinforced concrete buildings. *Journal of Structural Engineering*, **111**(4), 740–757,1985.

[11] Z.V. Milutinovic, G.S. Trendafiloski, Risk-UE: An advanced approach to earthquake risk scenarios with applications to different European towns. *Technical report, European Commission, WP4 Vulnerabilty of current buildings*, 2003.

[12] European Council, European macroseismic scale (EMS-98). *Cahier du Centre Européen de Géodynamique et de Sismologie*, G. Grünthal (Eds.), 1998.

[13] ASCE, *FEMA-356: Prestandard and commentary for the seismic rehabilitation of buildings.* 2000.

[14] M. Rota, A. Penna, C.L. Strobbia, Processing Italian damage data to derive typological fragility curves. *Soil Dynamics and Earthquake Engineering*, **28**, 933–947, 2008.

[15] M. Rota, A. Penna, G. Magenes, A methodology for deriving analytical fragility curves for masonry buildings based on stochastic nonlinear analyses. *Engineering Structures*, **32**, 1312–1323, 2010.

[16] N.N. Ambraseys, J. Douglas, R. Sigbjörnsson, C. Berge-Thierry, P. Sudaholc, G. Costa, P.M. Smit, *Dissemination of European Strong-Motion Data, vol. 2, using Strong-Motion Datascape Navigator*. CD-ROM collection, Engineering and Physical Science Reseach Council, United Kingdom, 2004.

[17] G. Pousse, L.F. Bonilla, F. Cotton, L. Margerin, Non-stationary stochastic simulation of strong ground-motion time-histories including natural variability: Application to the K-net Japanese database. *Bulletin of Seismological Society of America*, **96**(6), 2103–2117, 2006.

[18] F. Sabetta, A. Pugliese, Estimation of response spectra and simulation of non-stationary earthquake ground-motions. *Bulletin of Seismological Society of America*, **86**(2), 337–352, 1996.

[19] M. Shinozuka, M.Q. Feng, H. Kim, T. Uzawa, T. Ueda, Statistical analysis of fragility curves. *MCEER Technical Report*, Department of Civil and Environmental Engineering, University of Southern California, LA, USA, 2001.

[20] J. Douglas, *Selection of strong-motion records for use as input to the structural models of VEDA*. BRGM report RP-54584-FR, 2006.

[21] M. Shinozuka, Statistical analysis of bridge fragility curves. *US-Italy Workshop on Protective Systems for Bridges*, New-York, April 26-28, 1998.

[22] E. Parzen, On estimation of a probability density function and mode. *The Annals of Mathematical Statistics*, **33**, 1065–1076, 1962.

[23] B.R. Ellingwood, K. Kinali, Quantifying and communicating uncertainty in seismic risk assessment. *Structural Safety*, **31**, 179–187, 2009.